Research Article

L band brightness temperature observations over a corn canopy during the entire growth cycle

A.T. Joseph[1], R. van der Velde[2] P.E. O'Neill[1], B.J. Choudhury[1], R.H. Lang[3], E. Kim[1], T.Gish[4]

1. Hydrological Sciences Branch/614.3, Hydrospheric and Biospheric Sciences Laboratory, NASA/Goddard Space Flight Center, Greenbelt, MD 20771, USA, Tel.: 301-614-5804, Fax: 301 -614-5808, e-mail: Alicia.T.Joseph@nasa.gov, Peggy.E.ONeill@nasa.gov, Bhaskar.J.Choudhury@nasa.gov, Edward.J.Kim@nasa.gov

2. International Institute for Geo-Information Science and Earth Observation (ITC), Hengelsostraat 99, P.O. Box 6, 7500 AA Enschede, The Netherlands, Tel.:+ 31-53 4874327, Fax: + 31-53 4874400, e-mail: velde@itc.nl

3. Department of Electrical Engineering & Computer Sciences, the George Washington University, Washington, DC 20052, USA, Tel.: 202-994-6199, Fax: 202-994-0227, e-mail: lang@gwu.edu

4. USDA-ARS Hydrology and Remote Sensing Laboratory, Building 007, BARC-WEST, Beltsville, MD 20705, USA, Tel.: 301-504-8378, Fax: 301-504-8931, e-mail: Timothy.Gish@ars.usda.gov

* Corresponding author: Alicia T. Joseph (e-mail: Alicia.T.Joseph@nasa.gov)

Abstract: During a field campaign covering the 2002 corn growing season, a dual polarized tower mounted L-band (1.4 GHz) radiometer (LRAD) provided brightness temperature (T_B) measurements at preset intervals, incidence and azimuth angles. These radiometer measurements were supported by an extensive characterization of land surface variables including soil moisture, soil temperature, vegetation biomass, and surface roughness. During the period from May 22, 2002 to August 30, 2002 a range of vegetation water content (W) of 0.0 to 4.3 kg m^{-2}, ten days of radiometer and ground measurements were available. Using this data set, the effects of corn vegetation on surface emissions are investigated by means of a semi-empirical radiative transfer model. Additionally, the impact of roughness on the surface emission is quantified using T_B measurements over bare soil conditions. Subsequently, the estimated roughness parameters, ground measurements and horizontally (H)-polarized T_B are employed to invert the H-polarized transmissivity (γ_h) for the monitored corn growing season.

Keywords: Field campaign, L-band radiometry, vegetation effects, surface roughness

---

1. Introduction

Low frequency passive microwave observations have been intensively studied for their potential of retrieving soil moisture [e.g. 1-3]. Studies have demonstrated that when an appropriate characterization of vegetation, soil surface roughness and dielectric properties are applied, soil moisture can be retrieved fairly accurate from the brightness temperatures (T_B's) measured by microwave radiometers [e.g. 4,5]. As a result, the Soil Moisture and Ocean Salinity (SMOS [6]) mission is the first of three L-band radiometers designed for global soil moisture monitoring purposes to be launched. In the near future, the Aquarius and Soil Moisture Active Passive (SMAP [7]) missions will follow; their expected launch dates are in spring 2010 and in 2013, respectively. With this increased availability of low frequency spaceborne radiometer observations, new opportunities arise for monitoring soil moisture globally.

However, among the challenges in retrieving soil moisture from T_B measurements is to account for soil surface roughness and vegetation effects. Most retrieval approaches utilize similar radiative transfer equations [8-10]. These methods estimate the vegetation transmissivity (γ) using either multiple channel microwave data or ancillary data. Because the required ancillary data for global soil moisture retrieval applications may not be available at that scale, direct retrieval of the γ is preferred. However, the γ is polarization as well as wavelength (or frequency) dependent because the emitted radiation is differently attenuated as the orientation of the elements in the canopy layer changes relative to the wavelength and the direction of the polarization [e.g. 11-13]

Therefore, large scale soil moisture monitoring studies [e.g. 14-16] frequently adopt an ancillary data approach to determine the γ, which has been extensively described in the scientific literature [e.g.17, 18]. This characterization of the γ requires knowledge of the vegetation water content (W), and a crop-specific and frequency dependent empirical parameter b (elaborated below). The Normalized Difference Vegetation Index (NDVI) and related indices have been suggested as a surrogate for W in large-scale studies [e.g. 19, 20]. Then, the empirical parameter b should be implemented as a land cover specific parameter assigned based on a classification map.

Selection of the appropriate parameterization for a specific land cover relies, however, often on parameter sets derived from T_B measurements collected during past intensive field campaigns [e.g. 13,17]. By default, the validity of those parameterizations is restricted to the conditions for which they have been derived. Many of the past field campaigns covered, for example, a part of the growth cycle of agricultural crops. Therefore, the development of the γ and b parameter throughout the growth cycle is not fully understood.

This paper contributes to this understanding by analyzing the L-band H-polarized T_B's measured throughout the complete 2002 corn (Zea mays L.) growth cycle. The utilized data set has been collected at one of the fields of the Beltsville Agricultural Research Center (BARC) by an automated tower mounted L-band (1.4 GHz) radiometer (called LRAD) starting from May 22nd till the beginning of September. These radiometer measurements are supported by a detailed land surface characterization, which took place about once every week and included measurements of the vegetation biomass, soil moisture and soil temperature. Despite mechanical difficulties with scanning system of LRAD produced gaps in the data record, a total of ten days distributed over the growing

season of both radiometer and ground measurements are available covering a *W* range from 0.0 to 4.3 kg m^{-2}.

The objective of this investigation is to evaluate the variations in the γ and the empirical parameter *b* over the monitored corn growth cycle. To this aim, first, the impact of the surface roughness on the surface emission is quantified using the LRAD T_B's over bare soil conditions and an older data set collected at the BARC facility. Subsequently, the γ (and *b* parameter) are inverted from individual T_B measurements using the estimated roughness parameterization, and measured soil moisture and soil temperature. In addition, an analysis is presented of the sensitivity of the derived *b* parameters for uncertainties in the LRAD T_B and the assigned single scattering albedo (ω).

2. Theoretical background

The starting point for the computation of microwave emission from vegetated surfaces is the semi-empirical radiative transfer approach by Mo et al. [21], which is based on the assumption that at L-band attenuation is more dominant than scattering,

$$T_B^p = \left(1+R_s^p\gamma_p\right)\left(1-\gamma_p\right)\left(1-\omega_p\right)T_v + \left(1-R_s^p\right)\gamma_p T_s \tag{1}$$

where, T_B^p is the polarized brightness temperature, R_s^p is the soil surface reflectivity (= 1-emissivity), γ_p is the transmissivity of vegetation, ω_p is the single scattering albedo, T_s and T_v are the soil and canopy temperatures, respectively, and superscript and subscript *p* indicates polarization.

The first term on the right hand side of Eq. (1) represents the microwave emission directly by vegetation and the radiation emitted by the vegetation reflected by the soil surface back towards the sensor. The second term quantifies the emission contribution from the soil, corrected for the energy absorbed by the vegetation layer.

The solution to the radiative transfer equation requires parameterization of the vegetation and soil surface layer radiative transfer properties. Further, temperatures of the vegetation and soil surface layer are required. However, when assuming the vegetation and soil surface are in thermal equilibrium with each other, T_s and T_v can be considered equal; this condition occurs typically near dawn. The required temperature is then considered representative for the emitting layer.

2.1 Emission from soil

The surface emissivity is typically described in terms of the surface reflectivity. This is convenient because the microwave reflectivity under smooth surface conditions can be theoretically derived from Maxwell's equations (the Fresnel reflectivity). Fresnel reflectivity (R^p) for H- and V-polarizations for smooth soil surface are given as follows,

$$R^H\left(\theta\right) = \left|\frac{\cos\theta - \left(\varepsilon_r - \sin^2\theta\right)^{\frac{1}{2}}}{\cos\theta + \left(\varepsilon_r - \sin^2\theta\right)^{\frac{1}{2}}}\right|^2 \quad \text{and} \quad R^V\left(\theta\right) = \left|\frac{\varepsilon_r\cos\theta - \left(\varepsilon_r - \sin^2\theta\right)^{\frac{1}{2}}}{\varepsilon_r\cos\theta + \left(\varepsilon_r - \sin^2\theta\right)^{\frac{1}{2}}}\right|^2 \tag{2}$$

where, ε_r is the dielectric constant of soil, θ is the incidence angle.

In this study, the approach described by Wang and Choudhury [22] has been adopted to account for the effect of surface roughness on the reflectivity. This approach involves two parameters, where one parameter has an attenuating effect on the surface reflectivity and the other accounts for the depolarizing effect of the surface roughness,

$$R_s^p(\theta) = \left[(1-Q) R^p + Q R^q \right] \exp\left(-h\, G(\theta)\right) \tag{3}$$

where, h is roughness parameter given by $4k^2\sigma^2$ with k as the wavenumber ($2\pi/\lambda$) and σ as the root mean square (*rms*) height of the surface height variations, Q is a polarization mixing factor, $G(\theta)$ is a function describing the view angle dependency of the h parameter and superscript q represents the polarization orthogonal to polarization p, which can be either horizontal (H) or vertical (V).

Originally, Wang and Choudhury [22] took the function $G(\theta)$ equal to $\cos^2\theta$. However, Wang et al. [23] have found that the dependence of $\cos^2\theta$ is much too strong and replaced it by $G(\theta) = 1.0$ for best fitting their data. The latter is initially adopted here.

2.2 Vegetation effects on soil surface emission

Within the radiative transfer approach, vegetation effects are characterized by two parameters: transmissivity (γ) and single scattering albedo (ω). The ω is a measure for the amount of radiation scattered within the canopy and can be computed as follows,

$$\omega_p = \frac{\kappa_s^p}{\kappa_s^p + \kappa_a^p} \tag{4}$$

where, κ_s^p and κ_a^p are the scattering and absorption coefficients, respectively.

These scattering and absorption coefficients can be obtained through application of the discrete medium approach (Lang and Sidhu 1983, Chauhan 1997, and O'Neill et al. 1996), in which individual components of the vegetation layer (leaves and stems) are represented by elliptical and/or cylindrical dielectric scatterers. Alternatively, the ω is assumed to be negligible or a variable dependent on the growth stage, which can be determined from controlled experiments where all other variables (e.g. soil moisture, temperature of emitting layer, surface roughness and transmissivity) are measured.

The transmissivity describes the amount of soil emission passing through the vegetation layer and is an important variable for quantification of the effect of vegetation on microwave emission. The one-way transmissivity through the canopy layer is formulated as,

$$\gamma_p = \exp\left(\frac{-\tau_p}{\cos\theta} \right) \tag{5}$$

where, τ_p is the polarization dependent optical depth [12] or canopy opacity, which can be calculated using,

$$\tau_p = k_{ep} h_v \tag{5}$$

with

$$k_{ep} = \frac{4\pi}{\lambda} n_o \, \mathrm{Im}\left\langle f_{pp} \right\rangle \tag{6}$$

where, h_v is the canopy height, k_{ep} is a polarization dependent extinction coefficient, n_o is the number of phytoelements per unit volume, λ is the wavelength and $\mathrm{Im}\left\langle f_{pp} \right\rangle$ is the imaginary part of the polarization dependent scattering matrix.

Several studies [12,13,17] have shown that τ_p can be related to the vegetation water content as,

$$\tau_p = b_p \cdot W \tag{7}$$

where, W is the vegetation water content and b_p is an empirical parameter varying with crop type, canopy structure, wavelength, and polarization [12].

Eq. (7) for soil moisture retrieval requires information about vegetation class, W, and b_p parameters for different types of vegetation, and has been widely adopted and has been proposed as part of the soil moisture retrieval algorithms for current and future microwave radiometers [e.g. 24, 25].

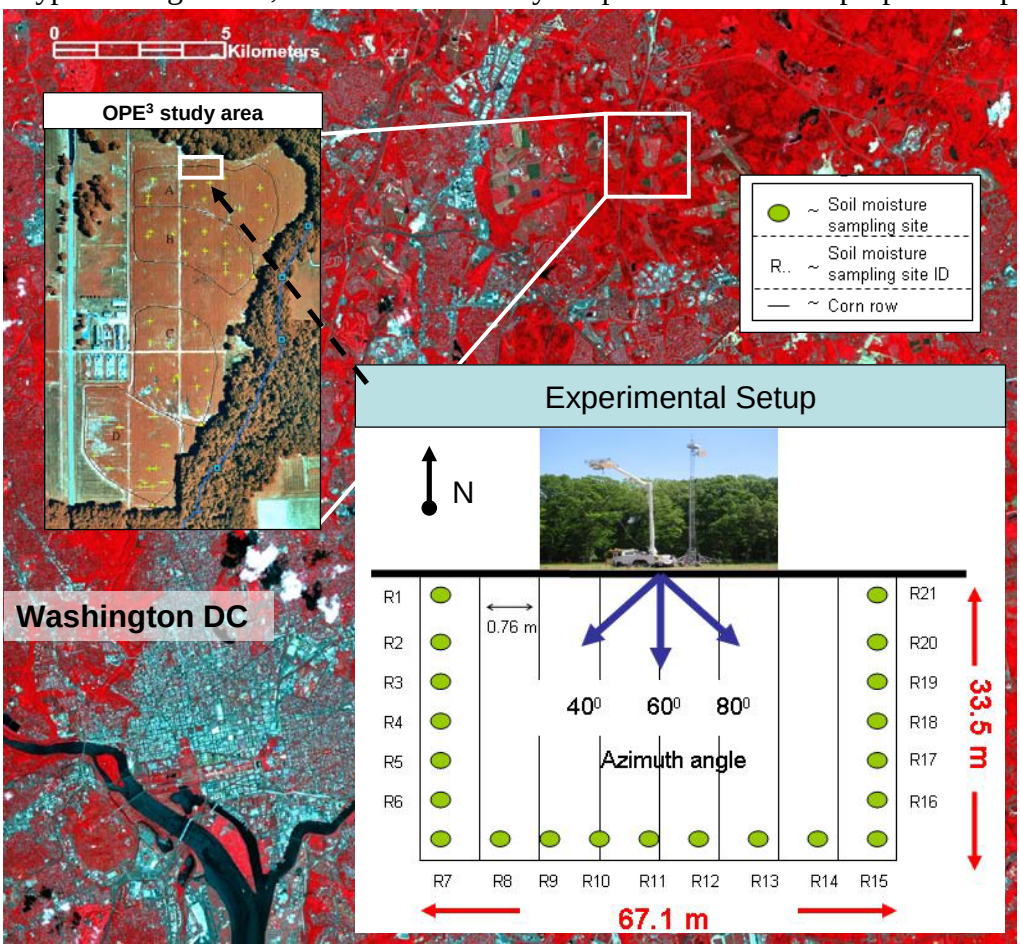

Figure 1. Location and schematization of the OPE[3] remote sensing experimental setup in 2002.

3. The OPE[3] experiment

3.1 Site description

The present study was conducted at Optimizing Production Inputs for Economic and Environmental Enhancement (OPE^3) test site managed by the USDA-ARS (United States Department of Agriculture-Agricultural Research Service) [26]. The site consists of four adjacent watersheds with similar surface and sub-surface soil and water flow characteristics and covers an area of 25 ha near Beltsville, Maryland (Figure 1). Each of the four watersheds is formed from sandy fluvial deposits and has a varying slope ranging from 1% to 4%. The soil textural properties are classified as sandy loam with 23.5% silt, 60.3% sand, 16.1% clay, and bulk density of 1.25 g cm^{-3}. A detailed description of the research activities can be found at http://hydrolab.arsusda.gov/ope3. (Verified December 23, 2009).

3.2 Ground measurements

The in-situ measurement strategy was designed to provide ground information to supplement the radar and radiometer data acquisitions, and took place every Wednesday, rainy days excluded. In this paper, an analysis of the radiometer observations is presented. A description of the radar data set is given in Joseph et al. [27].

During the field campaign (May 10 to October 2, 2002) representative soil moisture, soil temperature, vegetation biomass (wet and dry) and surface roughness measurements were taken around the radiometer footprints. Soil moisture and soil temperature measurements were collected at twenty-one sites located at the edge of a 67.1 m x 33.5 m rectangular area depicted in Figure 1. Vegetation biomass and surface roughness measurements were taken around the study area at representative locations.

Figure 2. (a) Comparison of the calibrated theta probe soil moisture against the gravimetrically determined soil moisture content converted to volumetric values. **(b)** Volumetric soil moisture (M_v) as measured by the theta probe, TDR and determined through a gravimetric sampling technique plotted against time.

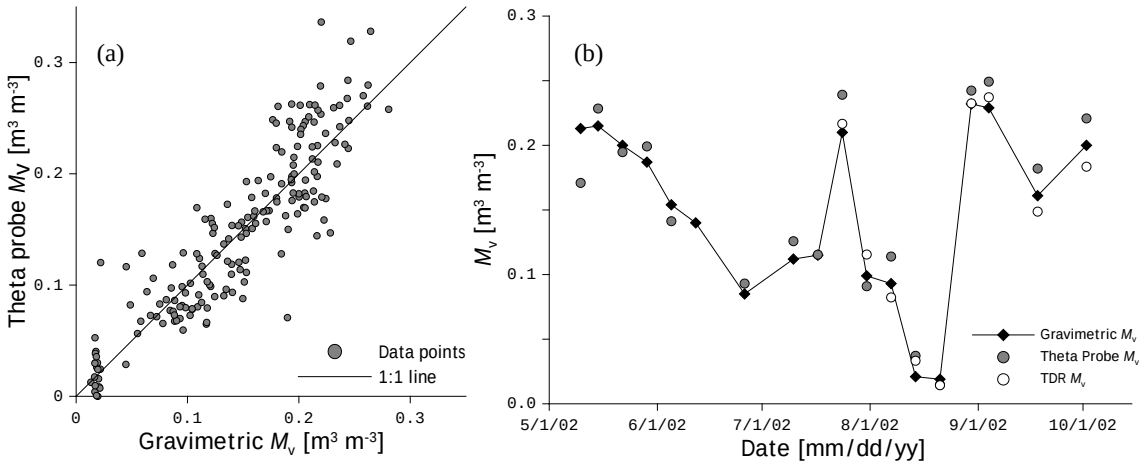

Soil moisture and Soil temperature

Soil moisture was measured using gravimetric, portable impedance probe (Delta-T theta probe[1]), and buried impedance probe (Time Domain Reflectometry (TDR)) techniques. Soil samples of the top

[1] The US Government does not endorse any specific brand of impedance probe for measuring soil moisture.

6-cm soil layer were collected at the beginning of each day in conjunction with the theta probe measurements primarily for calibration purposes. Theta probe measurements were collected typically at 8:00, 10:00, 12:00 and 14:00 hours (USA Eastern). The buried TDR probes were installed at locations R5, R11 and R18 (Fig. 1) at various depths (5, 10 and 20 cm) and insertion angles (horizontal, vertical, and 45 degrees).

Relative dielectric constant (ε_r) measured by the theta probe were converted to volumetric soil moisture (M_v) values by fitting a linear regression function through the following relationship (figure 2a),

$$\sqrt{\varepsilon_r} = a_0 + a_1 \cdot M_v \tag{8}$$

where, a_0 and a_1 are regression parameters. While general soil texture-specific parameters are available [28], a site specific calibration was performed. To achieve this, soil moisture determined gravimetrically from the soil samples was converted to M_v and used with concurrent probe observations to fit for each site a specific a_0 and a_1 parameter. Comparison of the calibrated theta probe M_v values with the gravimetric M_v (see Figure 2a) gives a root mean squared error (RSME) of 0.024 m^3 m^{-3}, which is comparable to calibration errors obtained with theta probe observations collected in several remote sensing campaigns [29]. In Figure 2b, the soil moisture observed by the three different measuring techniques are displayed as time series for comparison purposes. As shown in Figure 2b, the soil moisture values observed with the theta probe, gravimetric and TDR instruments are in agreement with each other, which justifies the use of each of their products.

Soil temperature measurements were taken manually at soil depths of 3- and 7-cm at each of the twenty-one sampling locations (annotated as R1 to R21 in Figure 1) throughout the experiment using Extech Instruments digital stem thermometers[2]. On intensive sampling days the soil temperatures were measured at 8:00, 10:00, 12:00, 14:00 hours, and the measurements on other days were taken approximately every two days at 8:00 and 14:00 hours.

Although the study area was selected to minimize the possible effects of land surface heterogeneity, small surface height and soil texture variations could potentially influence the representativeness of the measured soil moisture and temperature for the radiometer footprints. These effects are studied by evaluating the spatial soil moisture and temperature variability measured around the footprints. In Figures 3a and 3b, averages of the gravimetric M_v and soil temperature measured during the entire campaign are plotted for each site. Figure 3a shows that the western boundary (site R1-R6) is consistently wetter than the eastern boundary (site R16-R21). The difference between the maximum and minimum average soil moisture values observed in the study area is 0.04 m^3 m^{-3} (with 0.17 m^3 m^{-3} at site R9 and 0.13 m^3 m^{-3} at site R20). However, compared to the uncertainties in soil moisture measurements in general, see for example theta probe calibration uncertainty of 0.024 m^3 m^{-3}, this difference between the minimum and maximum averaged soil moisture is relatively small. We consider, therefore, the soil moisture variability around the radiometer footprint to be small and the mean of the twenty-one measurements representative for the radiometer footprint.

[2] The US Government does not endorse any specific brand of digital thermometers.

Figure 3. Averages of the gravimetric M_v **(a)** and soil temperature **(b)** measured during the entire campaign plotted for each sampling site separately. The site ID locations are shown in Figure 1 (R1 to R21). Error bars indicate the standard deviation in soil moisture or temperature measured throughout the campaign.

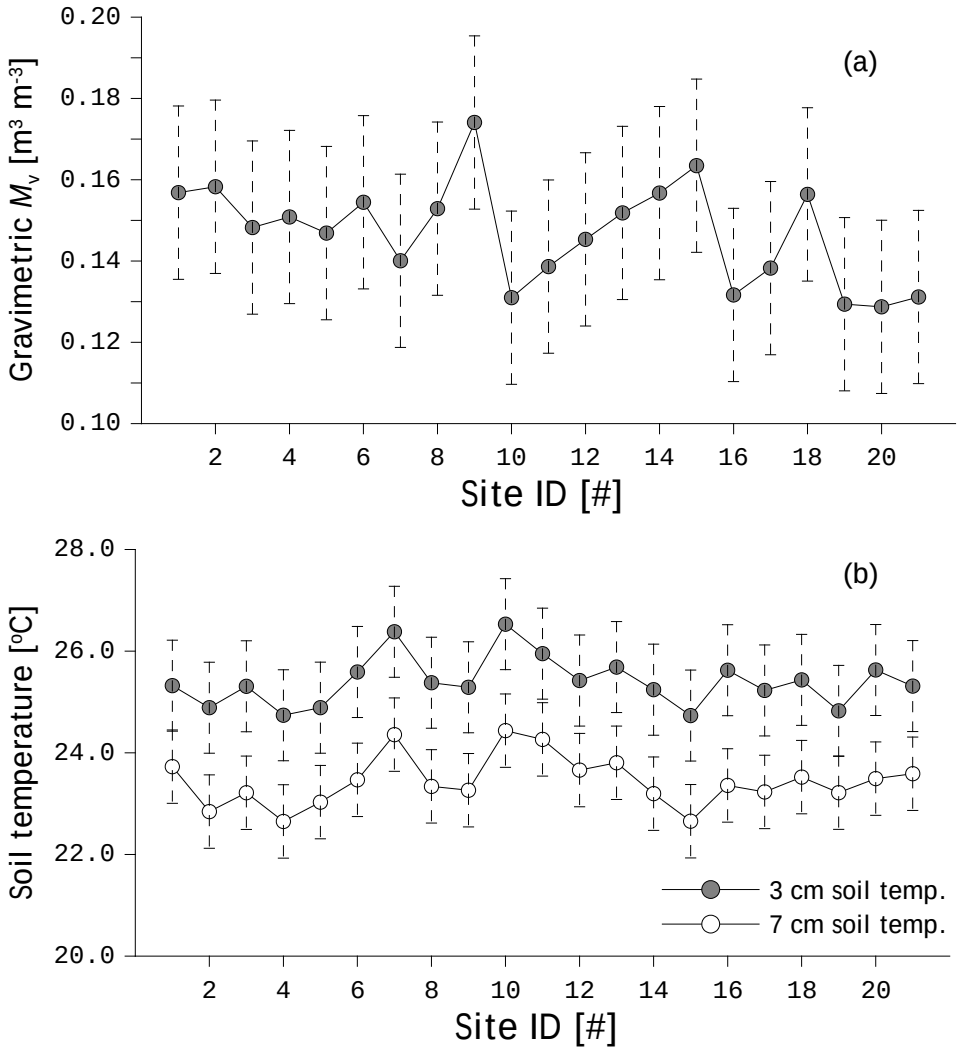

Vegetation

Corn was planted on April 17, reached peak biomass around July 24 and was harvested on October 2. Vegetation biomass and morphology were quantified through destructive measurements applied to 1 m^2 area (approximately 12 plants) once every week at 8:00 am. The water content, fresh and dry biomasses were determined separately for the individual plant constituents, such as leaves stems and cobs (when present).

Figure 4a shows the development biomasses and water content of the total plant over time and Figure 4b illustrates the temporal evolution of the water content in individual plant components. It follows from Figure 4b that in the beginning of the corn growing season, the canopy was primarily made up of leaves and stalks. In the middle of the growing season the stem contribution becomes more

dominant and cobs' water content increases to levels exceeding the leaf contribution. Near senescence, water content in the leaves is reduced further, whereas the contribution of the cobs to the total biomass remained constant.

Figure 4. (a) Total plant water content, fresh and dry biomass plotted against time. **(b)** Water content in the leaves, stems and cobs plotted against time. The markers indicate the dates at which measurements were made.

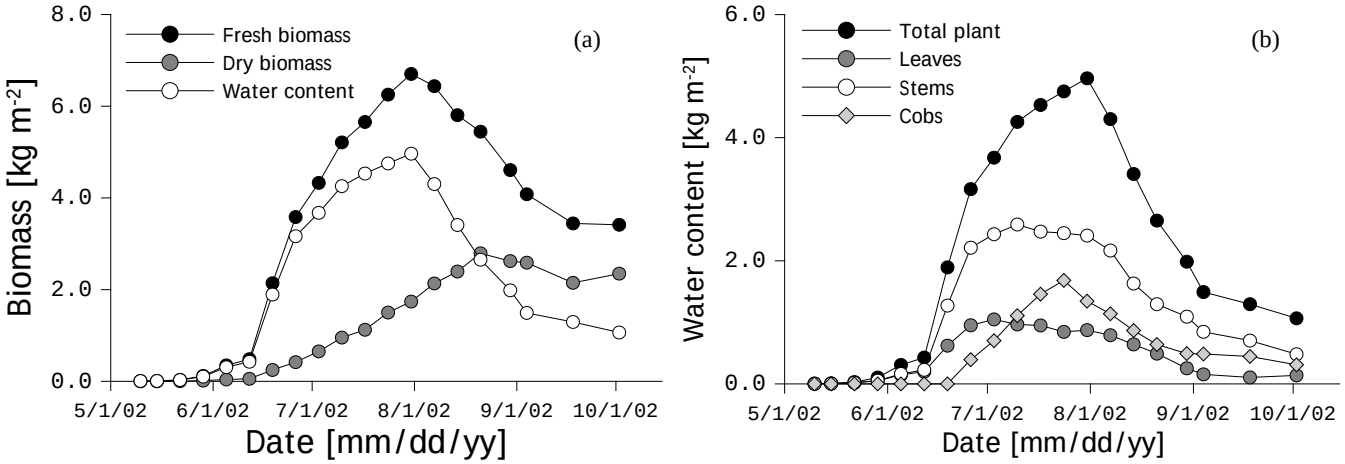

Surface roughness

During the experiment surface roughness was characterized on May 25 using the grid board technique. A 2-meter long grid board was placed in the soil and photographs were taken with the soil surface in front. In total, ten surface height profiles were recorded. The surface height profile in these pictures was digitized at a 0.5-cm interval, from which two roughness parameters were derived: root the *rms* height and the correlation length (L). The averaged *rms* height and L for the ten observed surface roughness profiles were found to be 1.62 and 12.66 cm, respectively. Figure 5 shows an example of a photograph taken for this roughness characterization and lists the roughness parameters calculated from the digitized surface height profiles.

Figure 5. The left panel shows an example of a picture taken for surface roughness characterization and the right panel lists the derived surface roughness parameters.

List of surface roughness parameters derived from digitized surface height profiles		
	***rms* height [cm]**	***L* [cm]**
Profile 1	1.11	5.18
Profile 2	0.81	6.35
Profile 3	0.95	6.39
Profile 4	0.75	3.22
Profile 5	0.74	4.52
Profile 6	2.35	8.95
Profile 7	2.46	12.20
Profile 8	1.95	10.75
Profile 9	1.91	8.16
Profile 10	1.68	6.84

3.3 Radiometer

The deployed radiometer was a dual-polarized (horizontal (H) and vertical (V)) L-band passive microwave sensor, called LRAD. The instrument was mounted on a portable 18 m tower and was designed to collect data automatically (for this experiment every hour) at five incidence angles (25, 35, 45, 55, and 60 degrees) and three azimuth angles over a range of 40 degrees. LRAD had a 3 dB beam width of approximately 12 degrees, which corresponds to footprints varying from 4.5 to 15.5 meters for the 25 to 60 degrees incidence angle range. Mechanical difficulties with the scanning system restricted the LRAD data collection, and produced considerable gaps in the season-long record. Nevertheless, ten days of complete record (ground measurements and radiometer observations) were available for the present analysis.

Each LRAD data run consisted of a pre-calibration, a measuring sequence, and a post-calibration. During each of the two calibration periods one microwave observation was acquired from a microwave absorber target of known temperature (hot target) and one microwave observation was acquired of the sky (cold target), which has at L band an T_B of ~ 5 K (3 K cosmic background radiation and 2 K atmospheric contribution). These two so-called "hot" and "sky" target observations can be used to calibrate, through linear interpolation, the radiometer observations of the land surface using,

$$T_B^p = \frac{T_{hot} - T_{sky}}{U_{hot} - U_{sky}} U_p + T_{sky} - \frac{T_{hot} - T_{sky}}{U_{hot} - U_{sky}} U_{sky} \quad (9)$$

where T_B is the brightness temperature [K], T indicates the temperature [K] of the specified target and U represents the LRAD voltage observations [Volt] with subscripts *hot* and *sky* indicating the hot and *sky* target properties and superscript *p* pointing towards the polarization dependence of the brightness temperature, which is either horizontal (H) or vertical (V). For processing the LRAD measurements to T_B's the pre-calibration was used, while the post-calibration was only employed to detect anomalous values. The estimated uncertainty of the calibrated H-polarized T_B is about ± 1.0 K.

While measurements were also collected for vertical polarization, there remain some unresolved issues with respect to the calibration of these measurements. Thus, vertical polarization measurements are not being presented at this time.

4. Results

4.1 Surface roughness parameter estimation based on H-polarized observations

Within the model of Wang and Choudhury [22], the effects of the surface roughness is characterized by two variables: 1) modification of the reflectance (*h* parameter), and 2) redistribution of the H- and V-polarized emitted radiation (*Q* parameter). Since the data set under investigation currently includes only calibrated H-polarized T_B measurements, the *Q* parameter is omitted (i.e., $Q = 0$), which essentially reduces the surface emission algorithm to the one proposed by Choudhury et al. [30]. This formulation has been adopted previously in several other studies [i.e.14, 19]. Based on this assumption, the *h* parameter can be estimated from H-polarized T_B's measured over bare soil using,

$$\left[1-\frac{T_B^H}{T_s}\right]=\left[R^H(\theta)\right]\exp(-h) \tag{10}$$

where, T_B^H is the H-polarized brightness temperature, T_s is the soil temperature, R^H is the H-polarized Fresnel reflectivity. For the OPE[3] campaign, the LRAD observations started on May 22, when corn crops had just emerged and the total fresh biomass was less than 0.04 kg m^{-2}. The T_B's measured under these low biomass conditions (May 22) were used to estimate the *h* parameter. Unfortunately, due to mechanical difficulties with the LRAD scanning system, only microwave observations for viewing angles of 35, 45 and 60 degrees were available for this part of the experiment. The twenty-one 3 cm surface temperature measurements taken around the radiometer footprint are averaged and are adopted as T_s. The resulting *h* parameter values are given in Table 1.

Table 1. Surface parameters obtained through inversion of H-polarized TB observations acquired over bare soil conditions.

	View angle		
	35 degrees	45 degrees	60 degrees
h	0.300	0.238	0.172
h ·*sec* θ	0.366	0.336	0.344

The derived *h* parameters fall within the range that has been reported previously. Wang et al. [23] reported a 0.00-0.53 *h* parameter range for surfaces with a *rms* height varying from 0.21 to 2.55 cm for a similar setting Considering an averaged *rms* height of 1.62 cm was observed around the radiometer footprint, the *h* parameter values obtained from the LRAD observations appears reasonable.

An interesting observation is, however, the angular dependence of the *h* parameter. Over a view angle range from 35 to 60 degrees, the *h* parameter decreases from 0.300 to 0.172. A angular dependence is partly expected because when a radiometer observes the land surface at different angles surface roughness may have a different impact on the surface emission, while recognizing that Eq. (10) is also an approximation [30]. However, the angular dependence of the *h* parameter could also be a result from the assumption of $Q = 0$. The Fresnel reflectivities for the H- and V-polarization are both a function of the incidence angle; excluding one of the two polarization components, as is done by assuming $Q = 0$ in Eq.(3), induces an angular dependence of the *h* parameter.

4.2 Surface roughness parameter estimation based on dual-polarized T_B

The surface roughness parameter *h* from the present data set demonstrates an angular dependence that is equal to adopting $G(\theta) = \sec\theta$ (see Table 1). A limitation of the present data set is that only H-polarized T_B observations are available to some degree of confidence. Therefore, in order to retrieve the *h* parameter from these T_B values, *Q* was taken equal to zero, which might alter the angular dependency (mixing of polarization). To elaborate on these findings, dual polarized L-band (~1.4 GHz) radiometer data sets collected over bare soils within the general area of the present study [23] are utilized to invert *h* and *Q* simultaneously.

The methodology used to retrieve the *Q* and *h* parameters has been adopted from Wang and Choudhury [22], which is based upon the following two relationships,

$$X(\theta)=\frac{T_{NB}^{V}(\theta)-T_{NB}^{H}(\theta)}{1-\frac{1}{2}\left[T_{NB}^{V}(\theta)+T_{NB}^{H}(\theta)\right]}=2\left[\frac{R^{H}(\theta)-R^{V}(\theta)}{R^{H}(\theta)+R^{V}(\theta)}\right](1-2Q) \tag{11}$$

$$Y(\theta)=1-\frac{1}{2}\left[T_{NB}^{V}(\theta)+T_{NB}^{H}(\theta)\right]=\frac{1}{2}\left[R^{H}(\theta)+R^{V}(\theta)\right]\exp\left(-hG(\theta)\right) \tag{12}$$

where T_{NB}^{p} is the normalized brightness temperature for polarization p, according to T_{B}^{p}/T_{s}, $X(\theta)$ is the surface roughness coefficient for deriving the Q parameter, $Y(\theta)$ is the surface roughness coefficient for deriving the h parameter, Eq. (11) and (12) can be rewritten to give the Q and h explicitly resulting in,

$$Q=\left[1-\frac{X(\theta)}{2\left[P(\theta)\right]}\right]\Big/2 \qquad \text{and} \qquad P(\theta)=\left[\frac{R^{H}(\theta)-R^{V}(\theta)}{R^{H}(\theta)+R^{V}(\theta)}\right] \tag{13}$$

with

$$h=-\frac{\ln\left[\dfrac{2Y(\theta)}{\left[R^{H}(\theta)+R^{V}(\theta)\right]}\right]}{G(\theta)} \tag{14}$$

The data set described in Wang et al. [23] includes ground measurements of soil moisture and temperature observed at various depths: 0-0.5, 2.5-5.0, 5.0-10.0 cm for soil moisture and 1.25, 2.5, 7.5 and 15.0 cm for soil temperature. In addition, dual-polarized T_B observations were collected at view angles of 10, 20, 30, 40, 50, 60 and 70 degrees. These measurements have been collected over soil surfaces with different roughness characteristics. For this investigation, a smooth and a rough surface are included in the analysis with a measured *rms* height of 0.73 and 2.45 cm, respectively. Because the present data set includes radiometer observations for an incidence angle range between 35 and 60 degrees, only the T_B measured over the 20 to 60 degrees incidence angle range are utilized from the Wang et al. [23].

The extensiveness of the radiometer and ground measurements permits all unknowns in Eq. (13) and (14) to be derived, and allows the computation of surface roughness parameters Q and h. In analogy with the previous roughness computations, the soil moisture content integrated over 0-5.0 cm has been used to compute the relative dielectric constant and the soil temperature at 2.5 cm has been used to derive the normalized brightness temperature. The resulting h parameters are plotted as a function of the incidence angle for the rough and smooth bare soil surface in Figures 7a and 7b respectively, whereas the computed Q values are shown as a function of the incidence angle for both the rough and smooth surface in Figure 7c. The h-parameters shown in Figure 7a and 7b have been computed assuming three different $G(\theta)$ relationships, which are: $\cos^2\theta$, $\cos\theta$, and $G(\theta) = 1.0$.

Figure 7. *h*-parameter as a function of incidence angle calculated from dual-polarized L-band T_B's measured over **(a)** smooth bare soil surface and **(b)** rough bare soil surface. **(c)** *Q*-parameters as a function of the incidence angle for same smooth and rough surfaces.

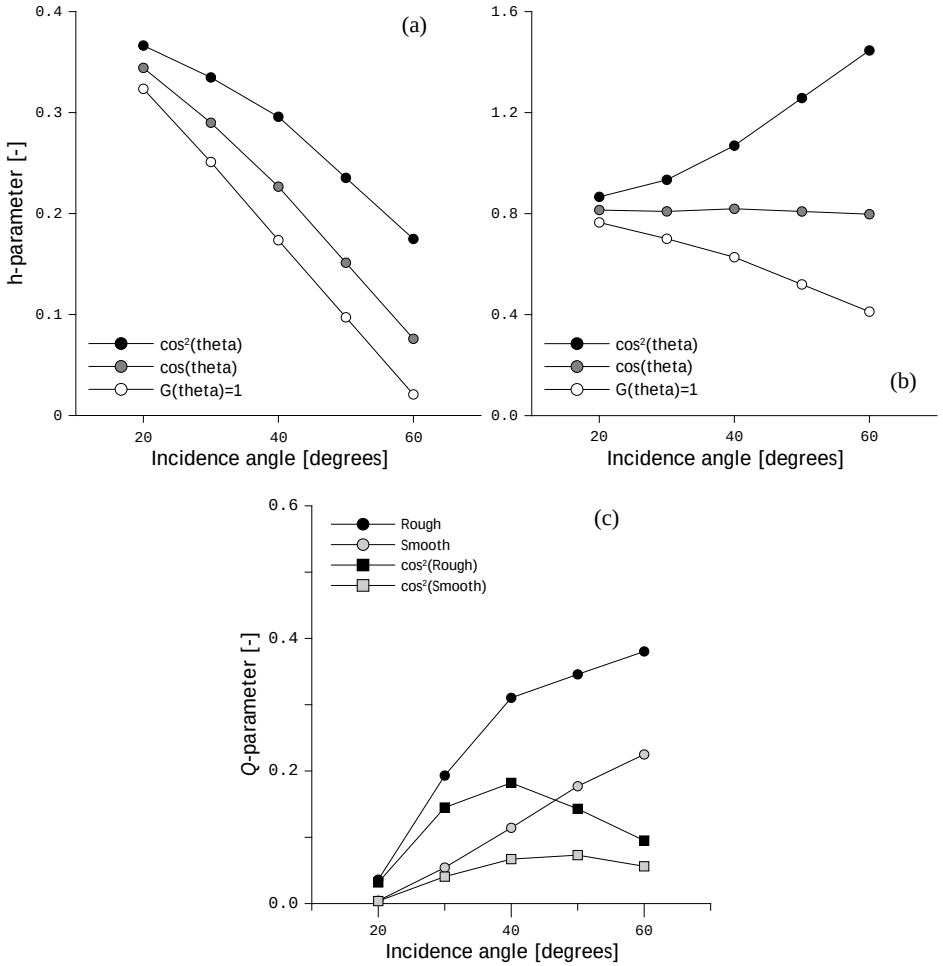

Figures 7a and 7b show a different angular behavior of the emission measured over the rough and the smooth surface. For the rough surface, it is observed that the function $G(\theta) = \cos\theta$ results in angular independent *h* parameter. However, none $G(\theta)$ functions are not able to suppress the angular dependence of the *h* parameter from the smooth surface, while $G(\theta) = \cos^2\theta$ provides the best approximation. Further, an angular dependency of *Q* parameter is noted in Figure 7c for both the rough and smooth surface. As shown in Figure 7c, the response of *Q* to incidence angle is, however, reasonably well approximated by

$$Q = Q(\theta)\cos^2(\theta) \tag{15}$$

During the OPE[3] campaign an average *rms* height of 1.62 cm was measured. As such, the roughness conditions can be considered as rougher than smooth surface, and as smoother than the rough surface of the Wang et al. [23] data set. Given that V-polarized component of surface reflectivity cannot be included in the *h* parameter retrieval from the present data set, the obtained function $G(\theta) = \cos\theta$ is assumed to be in agreement with the results obtained from the data set collected at OPE[3] in 2002. In addition, *Q* value of 0.1, being the average value of the *Q* derived for the rough and smooth surface, is utilized in combination with Eq. (15) to quantify depolarizing effects surface roughness. Then, using

these extrapolated parameterizations, the *h* parameter is inverted from the H-polarized T_B measurements on May 22.

The resulting *h* parameters are given in Table 2, which range from 0.165 to 0.171 and display, thus, no angular dependency. This illustrates that incorporation of V-polarized reflectivity (and $Q \neq 0.0$) is required for the *h* parameters to be valid over all incidence angles, which will be particularly important for retrieving soil moisture from the multi-angular data as is acquired by SMOS and will be the case for Aquarius. These values for the *h* parameter are used for the analysis of the H-polarized transmissivity.

Table 2. Surface parameters obtained through inversion of H-polarized T_B observations acquired over bare soil conditions with implementation of the *Q* parameter extrapolated from the Wang et al. [23] data set

	View angle		
	35 degrees	45 degrees	60 degrees
h	0.165	0.171	0.165

4.3 Estimation of the H-polarized transmissivity

When soil moisture and surface temperature are known, H-polarized transmissivity (γ_h) can be retrieved by assuming that temporal changes in the roughness parameterization are small and the single scattering albedo can be neglected. The γ_h is estimated for days, for which soil moisture, soil temperature measurements and radiometer observations are available. For this determination, the measured soil moisture is converted into the dielectric constant using the soil textural properties given in section 3.1 and the dielectric mixing model by Dobson et al. [31]. The measured soil temperature observed at a depth of 3-cm is used to correct the T_B observations for the changes in temperature of the soil-vegetation medium. Using this parameterization, the γ_h is computed using Eq. (1) for incidence angles of 35, 45 and 60 degrees.

Table 3. H-polarized transmissivities and *b* parameters estimated over the 2002 corn growth cycle using multi angular brightness temperatures.

Date	***W***	***Transmissivity***			***B parameter***		
	kg m^{-2}	*35^o*	*45^o*	*60^o*	*35^o*	*45^o*	*60^o*
May 29, 2002	0.1	0.919	0.936	0.958	0.675	0.455	0.211
June 5, 2002	0.3	0.813	0.840	0.868	0.554	0.401	0.230
June 19, 2002	1.9	0.803	0.844	0.800	0.095	0.063	0.059
June 26, 2002	3.1	0.782	0.788	0.741	0.063	0.053	0.047
July 3, 2002	3.7	0.807	0.803	0.743	0.039	0.037	0.037
July 9, 2002	4.2	0.763	0.739	0.711	0.055	0.053	0.041
July 12, 2002	4.3	0.793	0.757	0.726	0.045	0.046	0.037
August 21, 2002	2.6	0.840	0.812	0.763	0.055	0.056	0.051
August 30, 2002	2.0	0.838	0.835	0.795	0.073	0.069	0.058

The resulting γ_h are given for each day and for each of the three viewing angles in Table 3 and are plotted in Figure 8a against the *W* along with expected γ_h based on reported *b* parameter of 0.125 m^2

kg^{-1}. In addition, the LRAD *b* parameters are plotted against *W* in Figure 8b. Most *b* parameter values have been derived for dense corn canopies near peak biomass. Therefore, the comparison of *b* parameters derived for May 29 and June 5 (W = 0.1 and 0.3 kg m^{-2}) is not optimal. Since previous studies [e.g 17] have reported comparable *b* parameter for *W* range 1.2 – 6.0 kg m^{-2}, the field conditions observed on June 19 to August 30 (W = 1.9 – 4.3 kg m^{-2}) are comparable to corn canopies referred to in these previous investigations.

Figure 8. H-polarized corn transmissivities **(a)** and b parameters **(b)** inverted from LRAD T_B measured at incidence angle of 35, 45 and 60 degrees.

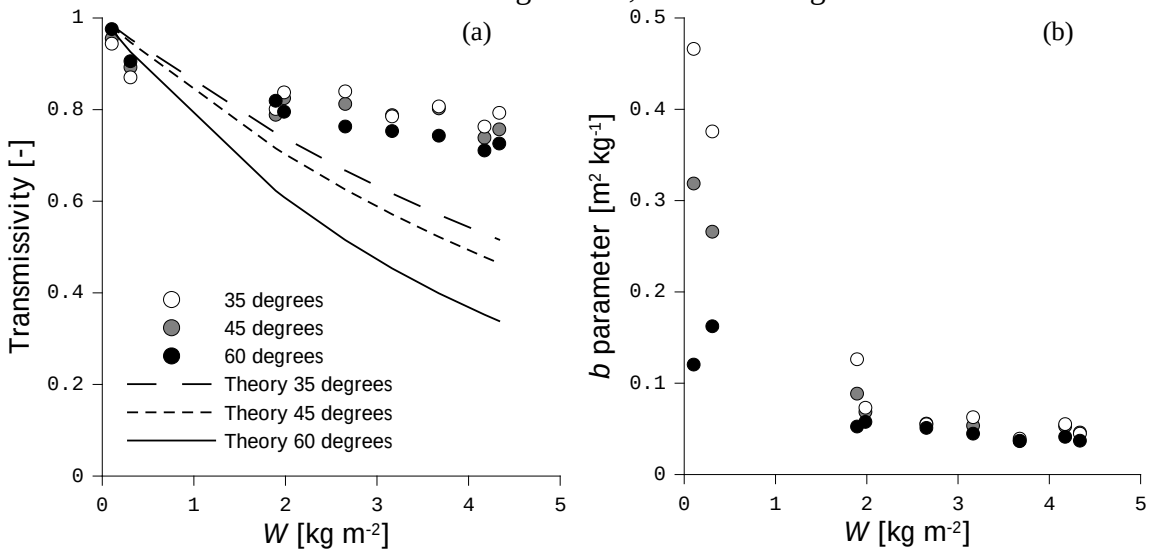

Figure 8a and 8b show that the LRAD γ_h follows a different pattern than is expected based on the literature reported *b* parameters. In the beginning of the corn growing season the γ_h is lower than expected, while closer to peak biomass the γ_h is larger. In terms of the *b* parameter, the results are much higher after the corn crops have just emerged and somewhat lower values at high *W* (> 1.9 kg m^{-2}). However, because at the beginning of the growing season the corn crops were small, the uncertainties in the *W* measurement can result in rather large deviations between the LRAD retrievals and literature reports. In addition, the contribution of the vegetation emission to the measured T_B is also small and, therefore, uncertainties in the T_B measurements (for example, stability of the instrument) can also be a cause for the obtained differences with the literature.

Table 4. H-polarized transmissivities and *b* parameters inverted from LRAD T_B measured on May 29, 2002 perturbed by ± 1.0 K.

	Transmissivity			***b-parameter***		
	35°	*45°*	*60°*	*35°*	*45°*	*60°*
TB-1.0 K	0.936	0.948	0.970	0.537	0.371	0.147
TB	0.944	0.955	0.976	0.466	0.319	0.120
TB+1.0 K	0.952	0.963	0.980	0.396	0.266	0.102

To illustrate the impact of the T_B uncertainties on the derived *b* parameter under low biomass conditions, the γ_h on May 29 has also been computed by perturbing the LRAD T_B with ± 1.0 K. The

obtained γ_h and b parameters are given in Table 4, which show that under low biomass conditions the sensitivity of the b parameter to uncertainties T_B is very high. When 1.0 K is added or subtracted from the LRAD T_B observations, the computed γ_h changes only about 0.007, while this changes the computed b parameter by 0.071 to 0.027 m^2 kg^{-1} depending on the incidence angle.

The high γ_h obtained from the T_B measured over more dense vegetation are most likely caused by scattering effects within the canopy, which has not been accounted for, since the ω = 0.0 has initially been assumed. At low frequencies and when the canopy attenuation is small, the ω value adopted within the radiative transfer approach is negligible (Jackson and O'Neill, 1990) because the vegetation emission is small, which would justify using ω = 0.0. As the biomass increases, however, the scattering within the canopy can have a significant impact on the measured T_B. In literature [32], reported ω values for corn canopies range from 0.04 to 0.13 for L band.

By assuming that the b parameter for corn vegetation at the OPE[3] site should be between 0.10 and 0.15 m^2 kg^{-1}, the ω's are computed for the LRAD measurements made on June 26. These ω computations have been made assuming b parameters of 0.10, 0.11, 0.12, 0.13, 0.14 and 0.15 m^2 kg^{-1}. The resulting ω's are given in Table 5, in which the numerical correlation between the b parameter and ω is demonstrated; for small b parameters, also ω is also small. Further, an angular dependency is noted among the inverted ω values. The derived values differ on average 0.025 between 35 and 45 degrees and 0.023 between 45 and 60 degrees. The angular dependence of ω is caused by the scattering within the complex canopy architecture (orientation of stems and leaves, as dielectric components of vegetation) [e.g. 33, 34]. Despite these observations, the LRAD inverted ω's in agreement with the parameter range documented in Van de Griend and Wigneron [32].

Table 5. Single scattering albedo (ω) inverted from LRAD T_B measured on June 26, 2002 (W = 3.1 kg m^{-2}) assuming a range b parameters from 0.10 to 0.15 m^2 kg^{-1}.

b-parameter m^2 kg^{-1}	***Single scattering albedo***		
	35°	*45°*	*60°*
0.10	*0.044*	*0.071*	*0.093*
0.11	*0.053*	*0.078*	*0.101*
0.12	*0.059*	*0.085*	*0.108*
0.13	*0.065*	*0.089*	*0.112*
0.14	*0.069*	*0.093*	*0.116*
0.15	*0.073*	*0.096*	*0.119*

5. Concluding remarks

In this investigation, the H-polarized T_B's measured by a tower mounted L-band (1.4 GHz) radiometer are used to analyze the vegetation effects on surface emission throughout the 2002 corn growth cycle. Concurrent with the radiometer measurements an extensive land surface characterization took place about once a week including soil moisture, soil temperature and vegetation biomass measurements. Over the period from May 22 to August 30, ten days with a complete record of ground and radiometer measurements are available for the present analysis that cover a vegetation water content (W) range of 0.0 to 4.3 kg m^{-2}.

The roughness parameter h, needed to correct for the effects of surface roughness, is inverted from H-polarized T_B measured early in the corn growing season over essentially an bare soil surface using the Choudhury et al. [30] surface emission algorithm assuming (Q = 0.0) and $G(\theta)$ equals 1.0. The h

parameters inverted using this formulation displays an unusual angular dependence. Analysis of a dual-polarized L-band radiometer data set from 1981 [23] demonstrates that the angular dependence of the *h* parameter in the present data set is partly caused by taking *Q* equal to 0.0. An alternative set of the *h* parameters was computed using the Wang and Choudhury (1981) surface emission algorithm ($Q \neq 0.0$) with *Q* parameter estimated from the 1981 data set as input.

Based on the derived Wang and Choudhury (1981) surface roughness formulation, the H-polarized corn transmissivities (γ_h) have been retrieved using the radiative transfer equation and assuming the single scattering albedo (ω_h) to be zero. The derived γ_h's are converted into *b* parameter values using the measured *W*. For sparse vegetation, the inverted γ_h's and *b* parameters were found to be larger than expected based on literature. It is, however, shown that under low biomass conditions when the emission by vegetation is small, uncertainties in T_B and *W* measurements result in a particularly large *b* parameter uncertainty. For dense vegetation, the inverted *b* parameters are somewhat smaller than expected, which is attributed to scattering within the canopy that is not accounted for since ω is initially assumed to be zero. Assuming the *b* parameter for corn varies between 0.10 and 0.15 [m^2 kg^{-1}], the ω_h has been computed from LRAD T_B measurements. For this range of *b* parameters, a range of ω_h values is found that is agreement with literature reports, but displays a strong angular dependence.

This study shows that the roughness parameters, *h* and *Q*, interact with each other as is also the case for the vegetation parameters, γ_h and ω_h. These interactions, together with any existing uncertainty in T_B need to be considered for estimating soil moisture. Moreover, the temporal variation observed among the computed γ_h's suggests that the empirical parameter *b* could also depend on the growth stage. Analysis of additional radiometer data sets and simulations by advanced vegetation scattering models is recommended to further improve the understanding of the behavior of the *b* parameters during the growth cycle.

Acknowledgements

The authors would like to acknowledge that the field campaign was financially supported through NASA and we would like to thank various students for participating in the field campaign.

References and Notes

1. Jackson, T.J. Measuring large scale surface soil moisture using passive microwave remote sensing. *Hydrological Processes* **1993**, *7*, 139-152.
2. Wigneron, J.P.; Kerr, Y.; Waldteufel, P.; Co-Authors. L-band microwave emission of the biosphere (L-MEB) model: description and calibration against experimental data sets over crop fields. *Remote Sensing of Environment* **2007**, *107*, 639-655.
3. Owe, M.; De Jeu, R.A.M. ; Holmes, T.R.H. Multi-Sensor Historical Climatology of Satellite-Derived Global Land Surface Moisture. *Journal of Geophysical Research* **2008**, *113*, F01002, doi:1029/2007JF000769.
4. Saleh, K.; Kerr, Y.H.; Richaume, P.; Escorihuela, M.J.; Panciera, R.; Delwart, S.; Boulet, G.; Maisongrande, P.; Walker, J.P.; Wursteisen, P.; Wigneron, J.P. Soil moisture retrievals at L-band using a two-step inversion approach. *Remote Sensing of Environment* **2009**, *113*, 1304-1312.

5. Panciera, R.; Walker, J.P.; Kalma, J.D.; Kim, E.J.; Saleh, K.; Wigneron, J.P. Evaluation of the SMOS L-MEB passive microwave soil moisture retrieval algorithm. *Remote Sensing of Environment* **2009**, *113*, 435-444.
6. Kerr, Y.H.; Waldteufel, P.; Wigneron, J.P.; Martinuzzi, J.M.; Font, J.; Berger, M. Soil moisture retrieval from space: The soil moisture and Ocean Salinity (SMOS) mission. *IEEE Transactions on Geoscience and Remote Sensing* **2001,** *39*, 1729-1735.
7. Entekhabi, D.; Njoku, E.G.; Houser, P.; Co-Authors. The Hydrosphere State (Hydros) mission: An Earth system pathfinder for global mapping of soil moisture and land freeze/thaw. *IEEE Transactions on Geoscience and Remote Sensing* **2004**, *42*, 2184-2195.
8. Jackson, T.J.; Le Vine, D.M.; Hsu, A.Y.; Oldak, A.; Starks, P.J.; Swift, C.T.; Isham, J.D.; Haken, M. Soil moisture mapping at regional scales using microwave radiometry: the Southern Great Plains hydrology experiment. *IEEE Transactions on Geoscience and Remote Sensing* **1999**, *GE-37*, 2136-2151.
9. Owe, M.; De Jeu, R.A.M.; Walker, J.P. A methodology for surface soil moisture and vegetation optical depth retrieval using the microwave polarization difference index. *IEEE Transactions on Geoscience and Remote Sensing* **2001**, *39*, 1643-1654.
10. Wen, J.; Su, Z.; Ma, Y. Determination of land surface temperature and soil moisture from Tropical Rainfall Measuring Mission/Microwave Imager remote sensing data. *Journal of Geophysical Research* **2003**, *108*, 4038-4050.
11. Jackson, T.J.; O'Neill, P.E. Attenuation of soil microwave emission by corn and soybeans at 1.4 and 5 GHz. *IEEE Transactions on Geoscience and Remote Sensing* **1990**, *28*, 978-980.
12. Wigneron, J.-P.; Calvet, J.-C.; De Rosnay, P.; Kerr, Y.; Waldteufel, P.; Saleh, K.; Escorihuela, M.J.; Kruszewski, A. Soil moisture retrievals from biangular L-band passive microwave observations. *IEEE Geoscience and Remote Sensing Letters* 2004, *1*, 277-281.
13 Van de Griend, A.A.; Wigneron, J.P. The b-factor as a function of frequency and canopy type at H-polarization. *IEEE Transactions on Geoscience and Remote Sensing*. **2004**, *42*, 1-10.
14. Drusch, M.; Wood, E.F.; Gao, H.; Thiele, A. Soil moisture retrieval during the Southern Great Plains Hydrology Experiment 1999: A comparison between experiment remote sensing data and operational products. *Water Resources Research* **2004**, *40*, W2504.
15. Cashion, J.; Lakshmi, V.; Bosch, D.; Jackson, T.J. Microwave remote sensing of soil moisture: evaluation of the TRMM microwave imager (TMI) satellite for the Little River Watershed Tifton, Georgia. *Journal of Hydrology* **2005**, *307*, 242-253.
16. Bindlish, R.; Jackson, T.J.; Gasiewski, A.; Stankov, B.; Klein, M; Cosh, M.H.; Mladenova, I.; Watts, C.; Vivoni, E.; Lakshmi, V.; Bolten, J.; Keefer, T. Aircraft based soil moisture retrievals under mixed vegetation and topographic conditions. *Remote Sensing of Environment* **2008**, *112*, 375-390.
17 Jackson, T.J.; Schmugge, T.J. Vegetation effects on the microwave emission of soils. *Remote Sensing of Environment* **1991**, *36*, 203-212.
18 Schmugge, T.J.; Jackson, T.J. A dielectric model of the vegetation effects on the microwave emission from soils. *IEEE Transactions on Geoscience and Remote Sensing* **1992**, *30*, 757-760.

19. Bindlish, R.; Jackson, T.J.; Wood, E.; Gao, H.; Starks, P.; Bosch, D.; Lakshmi, V. Soil moisture estimates from TRMM Microwave Imager observations over the Southern United States. *Remote Sensing of Environment* **2003**, *85*,507-515.
20. Jackson, T.J.; Chen, D.; Cosh, M.; Li, F.; Anderson, M.; Walthall, C.; Doriaswamy, P.; Hunt, E.R. Vegetation water content mapping using Landsat data derived normalized difference water index for corn and soybeans. *Remote Sensing of Environment* **2004**, *92*, 475-482.
21. Mo, T.; Choudhury, B.J.; Schmugge, T.J.; Wang, J.R.; Jackson, T.J. A model for microwave emission from vegetation-covered fields. *Journal of Geophysical Research* **1982**, *87*, 11229-11237.
22. Wang, J.R.; Choudhury, B.J. Remote sensing of soil moisture content over bare field at 1.4 GHz frequency. *Journal of Geophysical Research* **1981**, *86*, 5277-5282.
23. Wang, J.R.,; O'Neill, P.E.; Jackson, T.J.; Engman, E.T. Multifrequency measurements of the effects of soil moisture, soil texture, and surface roughness. *IEEE Transactions on Geoscience and Remote Sensing* **1983**, *GE-21*, 44-51.
24. Njoku, E.G. AMSR land surface parameters: surface soil moisture, land surface temperature, vegetation water content; Algorithm Theoretical Basis Documen. Jet Propulsion Laboratory: California Institute of Technology, Pasadena, CA, **1999**.
25. Kerr, Y. H.; Waldteufel, P.; Richaume, P.; Davenport, I.; Ferrazzoli, P.; Wigneron, J.P. SMOS level 2 processor Soil moisture Algorithm theoretical Basis Document (ATBD). SM-ESL (CBSA), CESBIO, Toulouse,SO-TN-ESL-SM-GS-0001, V5.a, 15/03/2006, **2006**.
26. Gish, T.J.; Walthall, C.L.; Daughtry, C.S.T.; Dulaney, W.P.; Mccarty, G.W. Watershed-Scale Sensing of Subsurface Flow Pathways at Ope3 Site. In: Proceedings of the First Interagency Conference on Research in the Watersheds, October 27-30, **2003**, Benson, Arizona. P. 192-197.
27. Joseph, A.T.; Van der Velde, R.; O'Neill, P.E.; Lang, R.H.; Gish, T. Soil moisture retrieval during a corn growth cycle using L-band (1.6 GHz) radar observations. *IEEE Transactions on Geoscience and Remote Sensing* **2008**, *46*, 2365-2374.
28. Miller, J.D.; Gaskin, G.D. Theta probe ML2x – principle of operation and applications, 2nd ed. Macaulay Land Use Research Institute (MLURI). Crairiebuckler, Aberdeen, AB158 QH, **1996**.
29. Cosh., M.H.; Jackson, T.J.; Bindlish, R.; Famiglietti, J.S.; Ryu, D. Calibration of an impedance probe for estimation of surface soil water content over large regions. *Journal of Hydrology* **2005**, *311*, 49-58.
30. Choudhury, B. J.; Schmugge, T. J.; Newton, R. W.; Chang, A. T. C. Effect of surface roughness on microwave emission of soils. *Journal of Geophysical Research* **1979**, *84*, 5699-5706.
31. Dobson, M.C.; Ulaby, F.T.; Hallikainen, M.T.; El-Rayes, M.A. Microwave dielectic behavior of wet soil – Part II: Dielectric mixing models. *IEEE Transactions on Geoscience and Remote Sensing* **1985**, *GE-23*, 35- 46.
32 Van de Griend, A.A.; Wigneron, J.P. On the measurement of microwave vegetation properties: Some guidelines for a protocol. *IEEE Transactions on Geoscience and Remote Sensing* **2004**, *42*, 2277-2289.
33. Lang, R.H.; Sidhu, J.S. Electromagnetic backscattering from a layer of vegetation: a discrete approach. *IEEE Transactions on Geoscience and Remote Sensing* **1983**, *21*, 62-71.

34. Chauhan, N.S. Soil moisture estimation under a vegetation cover: combined active passive microwave remote sensing approach. *International Journal of Remote Sensing* **1997**, *18*, 1079-1097.